Inorganic Chemistry

Article

pubs.acs.org/IC

Single-Crystal Growth and Size Control of Three Novel Polar Intermetallics: $Eu_{2.94(2)}Ca_{6.06}In_8Ge_8$, $Eu_{3.13(2)}Ca_{5.87}In_8Ge_8$, and $Sr_{3.23(3)}Ca_{5.77}In_8Ge_8$ with Crystal Structure, Chemical Bonding, and Magnetism Studies

Hyein Woo,[†] Gnu Nam,[†] Eunyoung Jang,[†] Jin Kim,[‡] Yunho Lee,[‡] Kyunghan Ahn,[§] and Tae-Soo You*[,†]

[†]Department of Chemistry, Chungbuk National University, Cheongju, Chungbuk 361-763 South Korea

[‡]Department of Chemistry, Korea Advanced Institute of Science and Technology, Daejeon, 305-701 South Korea

[§]Materials Research Center, Samsung Advanced Institute of Technology, Yongin-si, Gyeonggi-do 446-712 South Korea

Supporting Information

ABSTRACT: Three new quaternary polar intermetallic compounds of $Eu_{2.94(2)}Ca_{6.06}In_8Ge_8$, $Eu_{3.13(2)}Ca_{5.87}In_8Ge_8$, and $Sr_{3.23(3)}Ca_{5.77}In_8Ge_8$ have been synthesized by a metal-flux method using molten indium metal as a reactive flux, and the novel isotypic crystal structures have been characterized by both powder and single-crystal X-ray diffractions. All compounds crystallize in the orthorhombic space group *Pmmn* (Z = 2, Pearson symbol *oP*50) with 14 crystallographically unique atomic positions in the asymmetric unit. The lattice parameters are refined as follows: a = 36.928(2) Å, b = 4.511(1) Å, and c = 7.506(1) Å for $Eu_{2.94(2)}Ca_{6.06}In_8Ge_8$; a = 37.171(19) Å, b = 4.531(2) Å, and c = 7.560(4) Å for $Eu_{3.13(2)}Ca_{5.87}In_8Ge_8$; and a = 37.350(2) Å, b = 4.550(3) Å, and c = 7.593(4) Å for $Sr_{3.23(3)}Ca_{5.77}In_8Ge_8$. In particular, single crystals of two Eu-containing compounds are obtained as bundles of bar/needle-shaped crystals, and the thicknesses of those crystals can be controlled in the range between ca. 300 μm and ca. <10 μm by adjusting several reaction conditions, including the reaction cooling rate and the centrifugation temperature. The overall crystal structure is illustrated as an assembly of (1) the three-dimensional anionic framework, which is formed by the chains of edge-sharing $InGe_4$ tetrahedra and the annulene-like "12-membered anionic rings" connected via Ge_2 dimers, and (2) the cationic mixed sites embedded in the space between the anionic frameworks. Theoretical investigations based on tight-binding linear muffin-tin orbital (TB-LMTO) calculations provide a comprehesive understanding of the overall electronic structure and chemical bonding observed among anionic components and between anions and cations. Electron localization function (ELF) and electron density map present chemical bond strengths and polarization within the anionic framework. Magnetic susceptibility measurement proves an antiferromagnetic (AFM) ordering of Eu atoms below 4 K with a reduced effective magnetic moment of 7.12 μ_B for the Eu atom.

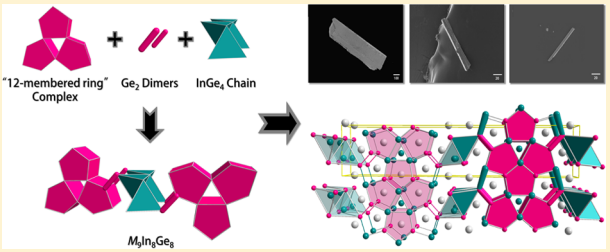

INTRODUCTION

The flux reaction using molten metals for the synthesis of new intermetallics or crystal growth of known compounds has been proven as a versatile synthetic toolbox for solid-state chemists for decades.[1−7] Other conventional synthetic methods for intermetallic compounds, such as arc melting or high-frequency induction heating, require very high reaction temperature,[8−10] and, given this limitation of synthetic environment, intermetallic compounds obtained from those conventional methods mostly crystallize in their high-temperature phases.[9−11] In addition, heating the reactants at very high temperature, followed by instantaneous quenching, does not provide an optimum condition for a product to grow single crystals that are large enough to be suitable for physicochemical analysis.[12] On the other hand, the flux reaction using molten metals as a solvent can sufficiently lower the maximum reaction temperature, resulting in providing a proper reaction environment to produce novel intermetallic compounds, which can be obtained only at the sufficiently low reaction temperature.[1−3,13−15]

Europium-containing polar intermetallics have been in our research interests, because of the potentially interesting magnetic property caused by the half-filled 4*f* orbitals of Eu^{2+} ions.[11,16,17] In addition, a Eu atom acting as a cation in polar intermetallics only partially transfers its valence electrons to anionic components, unlike that in traditional Zintl phases,[18−21] which results in forming a pseudo-gap at the Fermi level (E_F). These particular features can eventually lead to some interesting changes of magnetic characteristics of Eu^{2+} ions influencing other chemical and physical properties of given compounds.[16] In addition, we have also been interested in controlling the size of single crystals by adjusting various

Received: February 13, 2014
Published: April 22, 2014

   dx.doi.org/10.1021/ic500340x | Inorg. Chem. 2014, 53, 4669−4677

Table 1. Single-Crystal Crystallographic Data and Structure Refinement Results for $Eu_{2.94(2)}Ca_{6.06}In_8Ge_8$, $Eu_{3.13(2)}Ca_{5.87}In_8Ge_8$, and $Sr_{3.23(3)}Ca_{5.77}In_8Ge_8$[a]

	$Eu_{2.94(2)}Ca_{6.06}In_8Ge_8$	$Eu_{3.13(2)}Ca_{5.87}In_8Ge_8$	$Sr_{3.23(3)}Ca_{5.77}In_8Ge_8$
formula weight (fw), g mol^{-1}	2188.93	2210.74	2013.32
space group	*Pmmn* (No. 59)	*Pmmn* (No. 59)	*Pmmn* (No. 59)
Z	2	2	2
unit-cell dimension, Å	*a* = 36.928(2)	*a* = 37.171(19)	*a* = 37.350(2)
	b = 4.511(1)	*b* = 4.531(2)	*b* = 4.550(1)
	c = 7.506(1)	*c* = 7.560(4)	*c* = 7.593(1)
volume, Å^3	1250.47(11)	1273.3(11)	1290.55(13)
density (ρ_{calcd}), g cm^{-3}	5.814	5.766	5.181
absorption coefficient (μ), cm^{-1}	251.38	251.20	238.81
GOF on F^2	1.096	1.035	1.045
R [$I > 2\sigma(I)$]	R_1[b] = 0.0311	R_1[b] = 0.0318	R_1[b] = 0.0392
	wR_2 = 0.0545	wR_2 = 0.0598	wR_2 = 0.0833
R [all data]	R_1[b] = 0.0423	R_1[b] = 0.0485	R_1[b] = 0.0508
	wR_2 = 0.0593	wR_2 = 0.0660	wR_2 = 0.0911
largest diff. peak and hole, e$^-$ Å^{-3})	1.751 and −2.221	1.532 and −1.465	1.792 and −1.726

[a]Column heads show empirical expressions. [b]$R_1 = \sum||F_o| - |F_c||/\sum|F_o|$; $wR_2 = [\sum[w(F_o^2 - F_c^2]/\sum[w(F_o^2)^2]]^{1/2}$, where $w = 1/[\sigma^2F_o^2 + (AP)^2 + BP]$, and $P = (F_o^2 + 2F_c^2)/3$; *A* and *B* are weight coefficients.

reaction conditions under the metal-flux reactions,[22] just like many other chemical reactions using some types of organic solvents to grow single crystals.

In this report, we present three new quaternary polar intermetallic compounds of $Eu_{2.94(2)}Ca_{6.06}In_8Ge_8$, $Eu_{3.13(2)}Ca_{5.87}In_8Ge_8$, and $Sr_{3.23(3)}Ca_{5.77}In_8Ge_8$, which have been synthesized by the indium molten-metal flux method and crystallized in a novel isotypic structure type. The crystal structures of three title compounds were characterized by both powder and single-crystal X-ray diffraction (XRD) experiments. Large amounts of bundles of bar/needle-shaped single-crystals were obtained from the Eu-containing compounds, and the thickness of those crystals was successfully controlled in the micrometer scale by adjusting various reaction conditions. Comprehesive understandings about the electronic structure and chemical bonding of title compounds were attained by a series of theoretical calculations using tight-binding linear muffin-tin orbital (TB-LMTO)[23] method. Density of states (DOS) and crystal orbital Hamilton population (COHP) analyses[24] are also presented to evaluate the orbital interactions among individual components influencing local coordination geometries observed in the structure. Electron localization function (ELF) and electron density map calculated by these theoretical approaches also present chemical bond strengths and polarizations within the anionic framework. Magnetic susceptibility measurements and a magnetic ordering characteristics of Eu atoms in $Eu_{3.13(2)}Ca_{5.87}In_8Ge_8$ are also investigated.

EXPERIMENTAL SECTION

Synthesis and Crystal Growth. All sample preparation processes were conducted in an argon-filled glovebox with O_2 and H_2O contents of <0.1 ppm or under vacuum. Reactant elements were used as purchased from Alfa (Eu: ingot, 99.9%; Sr: granule, 99%; Ca: shot, 99.5%; In: tear drop, 99.99%; and Ge: pieces, 99.999%). The tanned surface of a Eu ingot was scrapped off by a scalpel just before being loaded into an alumina crucible. Title compounds were initially obtained from each reaction, respectively, using mixtures of elements in the ratio of Eu:Ca:Ge:In = 0.9:1.1:1:8 and Sr:Ca:Ge:In = 0.9:1.1:1:5. The excess amounts of In metals were used as a reactive self-flux. Stoichiometric mixtures of Eu, Ca, and Ge were loaded in a 2 cm^3 alumina crucible, and In was placed at the bottom and on the top of the element mixtures. The mixture of reactants containing Sr was loaded in a 2 cm^3 zirconia crucible to prevent Sr from reacting with a crucible made of alumina. After then, each reaction vessel was subsequently enclosed in a fused-silica ampule and flame-sealed under vacuum.

The fused-silica ampule was heated to 960 °C at the rate of 200 °C/h, and kept at this temperature for 20 h. At the final stage of the reaction process for the Eu-containing compounds, two reaction conditions, e.g., the reaction cooling rate and centrifugation temperature, varied between 5 °C/h and 100 °C/h and between 500 °C to 730 °C, respectively, in attempts to control the size of the single crystals. The mixture of reactants containing Sr produced only small cube-shaped single crystals from the reaction using the same reaction condition as the Eu analogue. Thus, we have not pursued additional synthesis any further for the Sr-containing compound to grow single crystals. The observed correlation between reaction conditions and the growth of single crystals will be thoroughly discussed in the subsequent Results and Discussion section. The extra amounts of molten In metals used as a solvent were removed by instantaneous centrifugation at the final stage of the reaction process, and large amounts of bundles of bar/needle-shaped single crystals with silver luster were obtained from the Eu-containing products. It should be noted that all attempts to synthesize the same crystal structure having only a single-type cation, either Eu, Sr or Ca, have failed under the above-mentioned reaction conditions, implying that the observed novel crystal structure should be stabilized only when both Eu (or Sr) and Ca coexist.[6] All compounds were air-/moisture-sensitive and started to decompose after 1 day.

X-ray Diffraction. Powder X-ray diffraction patterns were obtained using Bruker D8 diffractometer (monochromatic Cu Kα_1 radiation, λ = 1.54059 Å) with the step size of 0.05° in the range of 15° ≤ 2θ ≤ 85° with a total exposure time of 1 h. Primarily, the phase purity of each sample was briefly checked by comparing the collected powder patterns with a simulated pattern. For all Eu-containing samples synthesized under various reaction conditions, the collected powder patterns were compared each other to see whether there was any indication of peak shifting representing a deviation of chemical compositions. After that, the observed peaks were indexed using a program called Rietica[25] to evaluate the lattice parameters of each unit cell. The lattice parameters from powder XRD analyses match well with those obtained from single-crystal XRD analyses, and, because of a small difference of the Eu content between $Eu_{2.94(2)}Ca_{6.06}In_8Ge_8$ and $Eu_{3.13(2)}Ca_{5.87}In_8Ge_8$, nearly no significant peak shifting was observed between the collected powder patterns. Several peaks descended from the remaining indium metals were also indexed (see Figure S1 in the Supporting Information).

dx.doi.org/10.1021/ic500340x | Inorg. Chem. 2014, 53, 4669−4677

Table 2. Atomic Coordinates, Occupation Factors, and Equivalent Isotropic Displacement Parameters (U_{eq}) from Single-Crystal Structure Refinements for $Eu_{2.94(2)}Ca_{6.06}In_8Ge_8$, $Eu_{3.13(2)}Ca_{5.87}In_8Ge_8$, and $Sr_{3.23(3)}Ca_{5.77}In_8Ge_8$

atom	Wyckoff site	occupation factor	x	y	z	U_{eq}[a] (Å^2)
			$Eu_{2.94(2)}Ca_{6.06}In_8Ge_8$			
$M1$[b]	4*f*	0.285(2)/0.715	0.0456(1)	1/4	0.0084(1)	0.0068(2)
$M2$[b]	4*f*	0.508(2)/0.492	0.0754(1)	1/4	0.5209(1)	0.0063(2)
$M3$[b]	4*f*	0.260(2)/0.740	0.1442(1)	1/4	0.1497(1)	0.0061(2)
$M4$[b]	4*f*	0.269(2)/0.731	0.1740(1)	1/4	0.6671(1)	0.0063(2)
$M5$[b]	2*a*	0.294(3)/0.706	1/4	1/4	0.0313(1)	0.0066(3)
In1	4*f*	1	0.5171(1)	1/4	0.6500(1)	0.0063(1)
In2	4*f*	1	0.6110(1)	1/4	0.1630(1)	0.0086(1)
In3	4*f*	1	0.7040(1)	1/4	0.6867(1)	0.0068(1)
In4	2*b*	1	3/4	1/4	0.2845(1)	0.0075(1)
In5	2*a*	1	1/4	1/4	0.4556(1)	0.0087(2)
Ge1	4*f*	1	0.5250(1)	1/4	0.2668(1)	0.0056(2)
Ge2	4*f*	1	0.5866(1)	1/4	0.7880(1)	0.0058(2)
Ge3	4*f*	1	0.6344(1)	1/4	0.5425(1)	0.0059(1)
Ge4	4*f*	1	0.6897(1)	1/4	0.0511(1)	0.0061(2)
			$Eu_{3.13(2)}Ca_{5.87}In_8Ge_8$			
$M1$[b]	4*f*	0.307(4)/0.693	0.0455(1)	1/4	0.0082(2)	0.0149(5)
$M2$[b]	4*f*	0.532(4)/0.468	0.0753(1)	1/4	0.5208(1)	0.0151(4)
$M3$[b]	4*f*	0.281(4)/0.719	0.1442(1)	1/4	0.1495(2)	0.0148(5)
$M4$[b]	4*f*	0.289(4)/0.711	0.1739(1)	1/4	0.6666(2)	0.0147(5)
$M5$[b]	2*a*	0.315(5)/0.685	1/4	1/4	0.0313(2)	0.0154(7)
In1	4*f*	1	0.5170(1)	1/4	0.6503(1)	0.0156(2)
In2	4*f*	1	0.6109(1)	1/4	0.1630(1)	0.0202(2)
In3	4*f*	1	0.7038(1)	1/4	0.6863(1)	0.0158(2)
In4	2*b*	1	3/4	1/4	0.2849(2)	0.0167(3)
In5	2*a*	1	1/4	1/4	0.4550(2)	0.0190(3)
Ge1	4*f*	1	0.5249(1)	1/4	0.2675(2)	0.0145(3)
Ge2	4*f*	1	0.5866(1)	1/4	0.7876(2)	0.0153(3)
Ge3	4*f*	1	0.6343(1)	1/4	0.5433(2)	0.0153(3)
Ge4	4*f*	1	0.6897(1)	1/4	0.0513(2)	0.0140(3)
			$Sr_{3.23(3)}Ca_{5.77}In_8Ge_8$			
$M1$[b]	4*f*	0.441(10)/0.559	0.0459(1)	1/4	0.0096(2)	0.0146(6)
$M2$[b]	4*f*	0.549(10)/0.451	0.0759(1)	1/4	0.5223(2)	0.0126(5)
$M3$[b]	4*f*	0.224(11)/0.776	0.1446(1)	1/4	0.1512(3)	0.0113(7)
$M4$[b]	4*f*	0.276(10)/0.724	0.1739(1)	1/4	0.6688(2)	0.0114(6)
$M5$[b]	2*a*	0.246(14)/0.754	1/4	1/4	0.0311(3)	0.0100(9)
In1	4*f*	1	0.5174(1)	1/4	0.6495(1)	0.0128(2)
In2	4*f*	1	0.6117(1)	1/4	0.1600(1)	0.0187(2)
In3	4*f*	1	0.7040(1)	1/4	0.6866(1)	0.0132(2)
In4	2*b*	1	3/4	1/4	0.2840(2)	0.0137(3)
In5	2*a*	1	1/4	1/4	0.4555(2)	0.0141(3)
Ge1	4*f*	1	0.5243(1)	1/4	0.2687(2)	0.0120(3)
Ge2	4*f*	1	0.5872(1)	1/4	0.7861(2)	0.0112(3)
Ge3	4*f*	1	0.6349(1)	1/4	0.5428(2)	0.0120(3)
Ge4	4*f*	1	0.6901(1)	1/4	0.0497(2)	0.0117(3)

[a] U_{eq} is defined as one-third of the trace of the orthogonalized U_{ij} tensor. [b] M is refined as a statistical mixture of Eu (or Sr) and Ca.

Single-crystal XRD data were collected using Bruker SMART APEX2 CCD-based diffractometer equipped with Mo Kα_1 radiation (λ = 0.71073 Å) at room temperature. Several silvery lustrous bar/needle-shaped or cube-shaped crystals were isolated from bundles or aggregates of products selected from each batch of Eu- or Sr-containing compound, respectively. The crystal quality was initially checked by a rapid scan, and then the best crystal was chosen for the further data collection. Full data collection was processed using the Bruker APEX2 software.[26] Data reduction, integration, and unit-cell refinements were conducted using the SAINT program,[27] and semiempirical absorption correction based on equivalents was performed using the SADABS program.[28] The program XPREP in the SHELXTL software package was exploited to sort and merge the structure factors.[29] The crystal structures were solved by direct methods and refined to convergence by full matrix least-squares methods on F^2. Refined parameters include the scale factor, the atomic positions with anisotropic displacement parameters, extinction coefficients, and occupancy factors for five Eu(or Sr) and Ca mixed-sites. During the last refinement cycle, atomic positions were standardized using STRUCTURE TIDY.[30] Important crystallographic data, atomic positions, thermal displacement parameters, and selected interatomic distances are given in Tables 1−3. CIF files are deposited in Fachinformationszentrum Karlsruhe, 76344 Eggenstein-Leopoldshafen, Germany (fax: (49) 7247-808-666; E-mail: crysdata@fiz.karlsruhe.de) with depository numbers of CSD-427581 for $Eu_{2.94(2)}Ca_{6.06}In_8Ge_8$, CSD-427582 for $Eu_{3.13(2)}Ca_{5.87}In_8Ge_8$ and CSD-427583 for $Sr_{3.23(3)}Ca_{5.77}In_8Ge_8$.

dx.doi.org/10.1021/ic500340x | Inorg. Chem. 2014, 53, 4669−4677

Table 3. Selected Interatomic Distances for $Eu_{2.94(2)}Ca_{6.06}In_8Ge_8$, $Eu_{3.13(2)}Ca_{5.87}In_8Ge_8$, and $Sr_{3.23(3)}Ca_{5.77}In_8Ge_8$

	Distance (Å)		
atomic pair	$Eu_{2.94(2)}Ca_{6.06}In_8Ge_8$	$Eu_{3.13(2)}Ca_{5.87}In_8Ge_8$	$Sr_{3.23(3)}Ca_{5.77}In_8Ge_8$
In1−Ge1(×2)	2.809(1)	2.820(1)	2.827(1)
In1−Ge1 (×1)	2.891(1)	2.909(2)	2.903(2)
In1−Ge2	2.769(1)	2.788(2)	2.805(2)
In2−Ge1	3.270(1)	3.291(2)	3.366(1)
In2−Ge2	2.955(1)	2.978(2)	2.983(2)
In2−Ge3	2.977(1)	3.003(2)	3.034(2)
In2−Ge4	3.026(1)	3.047(2)	3.046(2)
In3−Ge3	2.788(1)	2.803(2)	2.803(2)
In3−Ge4	2.786(1)	2.809(2)	2.806(2)
In3−In5	3.020(1)	3.036(1)	3.048(1)
In4−Ge4	2.833(1)	2.855(2)	2.860(2)
In4−In5	2.982(1)	3.000(2)	3.015(1)
Ge2−Ge3	2.551(1)	2.559(2)	2.567(2)

Electronic Structure Calculations. Density functional theory (DFT) calculations for the idealized composition of "$Eu_3Ca_6In_8Ge_8$" were conducted using the Stuttgart TB-LMTO47 program with the atomic sphere approximation (ASA).[23d] Exchange and correlation were treated by the local density approximation (LDA).[23b] All relativistic effects except spin−orbit coupling were taken into account by using a scalar relativistic approximation. In the ASA method, space is filled with overlapping Wigner−Seitz (WS) atomic spheres,[23e] and the symmetry of the potential is considered spherical inside each WS sphere. A combined correction is used to take into account the overlapping part.[31] The radii of WS spheres were determined by an automatic procedure[31] and by requiring that the overlapping potential be the best possible approximation to the full potential.[31] This overlap should not be too large, because the error in kinetic energy introduced by the combined correction is proportional to the fourth power of the relative sphere overlap. No empty sphere[23e] was necessary. The used WS radii are listed as follows: Eu = 1.95−2.17 Å, Ca = 2.00−2.11 Å, In = 1.65−1.93 Å, and Ge = 1.48−1.61 Å. The basis sets included 6*s*, 6*p*, and 5*d* orbitals for Eu; 4*s*, 4*p*, and 3*d* orbitals for Ca; 5*s*, 5*p*, and 5*d* orbitals for In; and 4*s*, 4*p*, and 4*d* orbitals for Ge. The Eu 5*d*, Ca 3*d*, In 5*d*, and Ge 4*d* orbitals were treated by the Löwdin downfolding technique.[23e] The 4*f* wave functions of Eu were treated as core functions. The *k*-space integrations were conducted by the tetrahedron method,[32] and the self-consistent charge density was obtained using 343 irreducible *k*-points in the Brillouin zone for the orthorhombic unit cell.

EDS and SEM Analysis. Elemental analysis by energy-dispersive X-ray spectroscopy (EDS) and images of selected single crystals were taken using a ULTRA Plus field-emission scanning electron microscope (SEM) system with an acceleration voltage of 30 kV. Several bar/needle-shaped single-crystals of title compounds with different sizes were selected from each reaction batch synthesized under various reaction conditions, using the In metal-flux reaction. Selected single crystals were carefully mounted on the circumference of an aluminum puck with double-sided conducting carbon tapes in an argon-filled glovebox. EDS analysis indicated $Eu_{3.34(9)}Ca_{5.53}In_{8.27}Ge_{7.86}$ and $Sr_{3.30(9)}Ca_{5.57}In_{7.86}Ge_{8.27}$ for $Eu_{3.13(2)}Ca_{5.57}In_8Ge_8$ and $Sr_{3.23(3)}Ca_{5.77}In_8Ge_8$, respectively.

Magnetic Property Measurements. Magnetic properties were measured using vibrating sample magnetometry (VSM) (Quantum Design PPMS) performed on a polycrystalline sample of $Eu_{3.13(2)}Ca_{5.87}In_8Ge_8$ weighing ∼20−30 mg. For the dc magnetization measurements, a sample was initially cooled under zero magnetic field, and then the measurement was performed on heating from 4 to 300 K under an applied magnetic field of 10 kOe (zero-field-cooled condition, ZFC). The measurement was repeated upon heating with the magnetic field of 10 kOe turned on (field-cooled condition, FC). For the isothermal magnetization measurements, the sample was cooled under zero magnetic field, and the data were collected only at 4 K in dc magnetic fields varying from −70 kOe to 70 kOe.

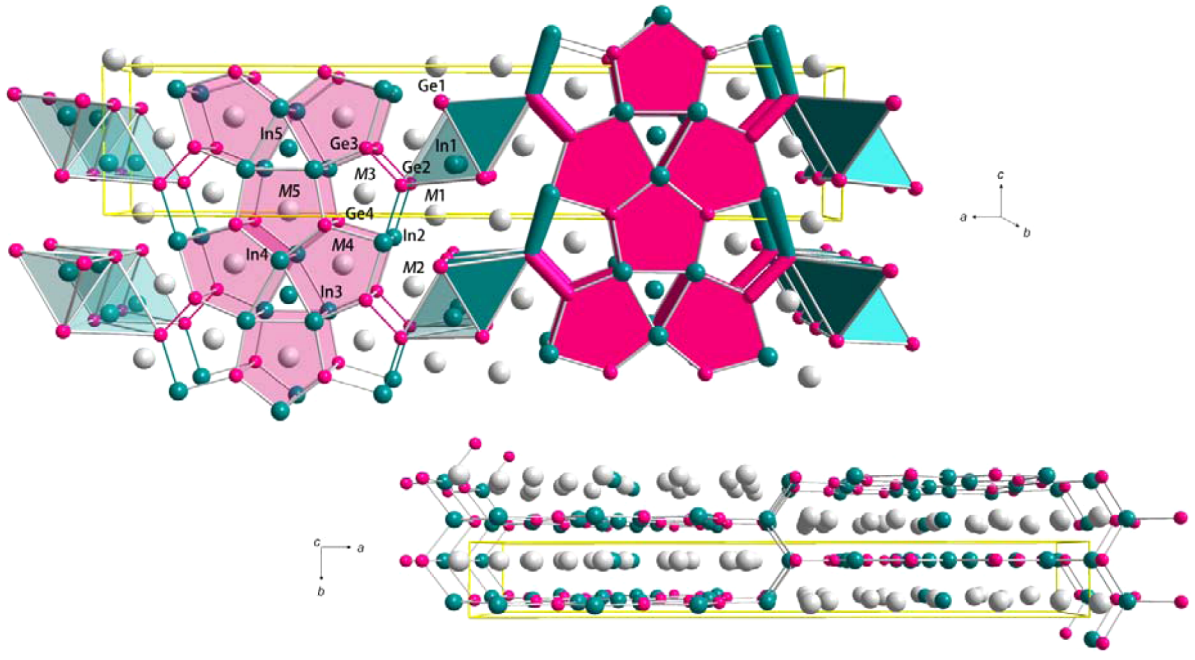

Figure 1. Combined ball-and-stick and polyhedral representations of the crystal structure of the orthorhombic $M_9In_8Ge_8$ (M = Eu/Ca- or Sr/Ca-mixed site) phase viewed down the *b*-axis (top) and the *c*-axis (bottom). The Ge_2 dimers and In−Ge bond connecting the "12-membered rings" and $InGe_4$ tetrahedra are highlighted in magenta and green, respectively. Unit cell is outlined in yellow. Color codes are as follows: M, gray; Ge, magenta; and In, green.

dx.doi.org/10.1021/ic500340x | *Inorg. Chem.* 2014, 53, 4669−4677

RESULTS AND DISCUSSION

Structural Description. Three compounds of $Eu_{2.94(2)}Ca_{6.06}In_8Ge_8$, $Eu_{3.13(2)}Ca_{5.87}In_8Ge_8$ and $Sr_{3.23(3)}Ca_{5.77}In_8Ge_8$ crystallized in the orthorhombic crystal system with a space group of *Pmmn* (Z = 2, Pearson code *oP*50) and adopted a novel crystal structure having 14 crystallographically independent atomic sites in the asymmetric unit, as shown in Figure 1. In particular, all five cationic sites contain the mixed occupations of Eu(or Sr) and Ca with various atomic ratios. Detail crystallographic information is given in Tables 1−3.

The isotypic crystal structure of three compounds can be viewed as a combination of the complex 3-D polyanionic framework and the mixed-cationic sites embedded in the polyanionic framework just as many other polar intermetallics and Zintl phases have already displayed.[5−7] In detail, the 3D polyanionic framework consisting of In and Ge can be illustrated as a simple assembly of two smaller structural moieties: (1) the one-dimensional (1D) chains of edge-sharing $InGe_4$ tetrahedra propagating through the crystallographic *b*-axis and (2) the distorted annulene-like "12-membered rings", in which In and Ge atoms are alternatively allocated. The similar tetrahedral-shaped $InGe_4$ conformation, which eventually forms the 1D chain by sharing two edges with neighbors, has been previously reported in some other rare-earth-metal-containing germanide phases. Those include $(Eu_{1-x}Ca_x)_3In_2Ge_3$ ($0.35 \le x \le 0.70$),[6] $(Eu_{1-x}Ca_x)_4In_3Ge_4$ ($0.78 \le x \le 0.90$),[6] and $RE_4Ni_2InGe_4$ (RE = Dy, Ho, Er, and Tm).[33] The observed In−Ge bond distances in the tetrahedron range of 2.769−2.909 Å. Although the observed interatomic distances are slightly longer than the sum of the covalent radii of two components (r_{In} = 1.55 Å and r_{Ge} = 1.22 Å),[34] those values still remain in the scope of the previously reported corresponding distances of two-center two-electron bond, such as 2.75−2.89 Å in $(Eu_{1-x}Ca_x)_4In_3Ge_4$ ($0.35 \le x \le 0.70$),[6] 2.760−2.869 Å in $(Eu_{1-x}Ca_x)_3In_2Ge_3$ ($0.78 \le x \le 0.90$),[6] 2.716−2.822 Å in $(Sr_{1-x}Ca_x)_3In_2Ge_4$ (x = 0.39, 0.49),[7] 2.672−2.877 Å in $Sr_{1.50}Ca_{3.50}In_3Ge_6$,[7] and 2.840−3.081 Å in $RE_4Ni_2InGe_4$ (RE = Dy, Ho, Er, and Tm).[33] The annulene-like "12-membered anionic ring" has been mentioned in an article about two Sm_3Ge_5−type polymorphs, in which the intercorrelation between two closely related, but clearly distinctive Ge frameworks in the RE_3Ge_5 (RE = Sm and Gd, α-Sm_3Ge_5 type) phase and $SmGe_2$ (AlB_2-type) were discussed.[5] In the report, the regular-fashioned Ge vacancies accompanied by some structural distortions on the 6^3 frameworks of $SmGe_2$ (AlB_2-type) could elucidate the formation of 12-membered rings observed in the RE_3Ge_5 (α-Sm_3Ge_5 type) phase. In our title compounds, the very similar distorted 12-membered ring can be derived through the same structural transformation of an imaginary 6^3 frameworks consisting of In and Ge as one imaginary Ge at the center of the 6^3 framework is removed. Two such neighboring rings can be viewed as if they are stacked on top of each other along the *a*-axis and eventually considered as a cluster of three two-edge-shared pentagonal-prisms surrounding three cationic sites, respectively. Therefore, the overall 3D polyanionic frameworks can be described as an extended structure consisting of two such 12-membered ring complexes and one $InGe_4$ chain connected via Ge_2 dimers, as illustrated in Figure 2.

The In−Ge distances of the 12-membered rings range from 2.786 Å to 3.047 Å, and the Ge−Ge bond distances of a connector are 2.551 and 2.559 Å. The In−Ge distances are also in very good agreements with some examples mentioned above, and the Ge−Ge distance matches well with examples listed below: 2.54 Å for $(Eu_{1-x}Ca_x)_4In_3Ge_4$ ($0.35 \le x \le 0.70$),[6] 2.527−2.533 Å for $(Eu_{1-x}Ca_x)_3In_2Ge_3$ ($0.78 \le x \le 0.90$),[6] 2.538−2.622 Å for $(Sr_{1-x}Ca_x)_3In_2Ge_4$ (x = 0.39, 0.49),[7] and 2.528−2.550 Å for $Sr_{1.50}Ca_{3.50}In_3Ge_6$.[7] It is noteworthy that the isotropic displacement parameters of the In2 site in all three compounds are slightly larger than those of other In sites. This type of relatively larger displacement parameters at a particular In site was previously reported by us for the $M_4In_3Ge_4$ and $M_3In_2Ge_3$ (M = Eu/Ca-mixed site) systems.[6] As discussed there, it should be attributed to the local coordination geometry around the In2 site, which is a distorted square-planar formed by four Ge atoms with elongated interatomic distances (2.955(1)−3.366(1) Å) rather than a tetrahedral coordination geometry.

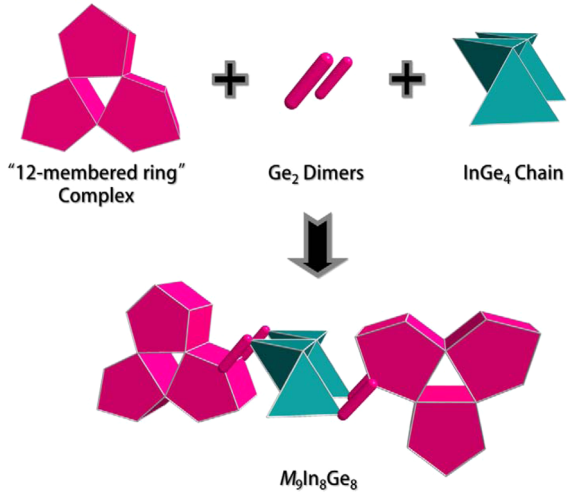

Figure 2. Schematic illustration showing the formation of the 3D polyanionic frameworks consisting of the annulene-like "12-membered rings" complex and the $InGe_4$ tetrahedral chain connected via Ge_2 dimers in the $M_9In_8Ge_8$ (M = Eu/Ca- or Sr/Ca-mixed site) phase.

Five symmetrically independent cationic sites are found between the 3D polyanionic frameworks (Figure 3). As mentioned earlier, all five sites show different Eu (or Sr) and Ca-mixed ratios varying from ca. 26% (22%) and 74% (78%) to ca. 53% (55%) and 47% (45%). In particular, M2, M3, M4, and M5 sites are located in the 10-coordinated pentagonal-prismatic environment, which are formed by six Ge and four In atoms for M2 and M3 sites, and four Ge and six In atoms for M4 and M5 sites, respectively. The M1 site is situated in a distorted square-pyramidal environment formed by five Ge atoms, in which four

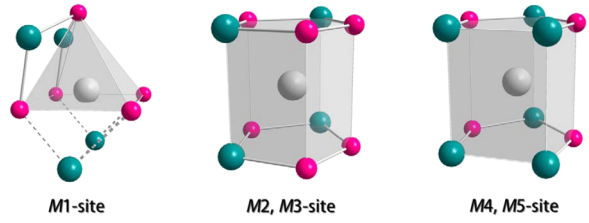

Figure 3. Five cationic sites in the $M_9In_8Ge_8$ (M = Eu/Ca- or Sr/Ca-mixed site) phase shown as coordination polyhedra with surrounding anionic atoms. Color codes: M, gray; Ge, magenta; and In, green (M = Eu/Ca- or Sr/Ca-mixed site).

dx.doi.org/10.1021/ic500340x | Inorg. Chem. 2014, 53, 4669−4677

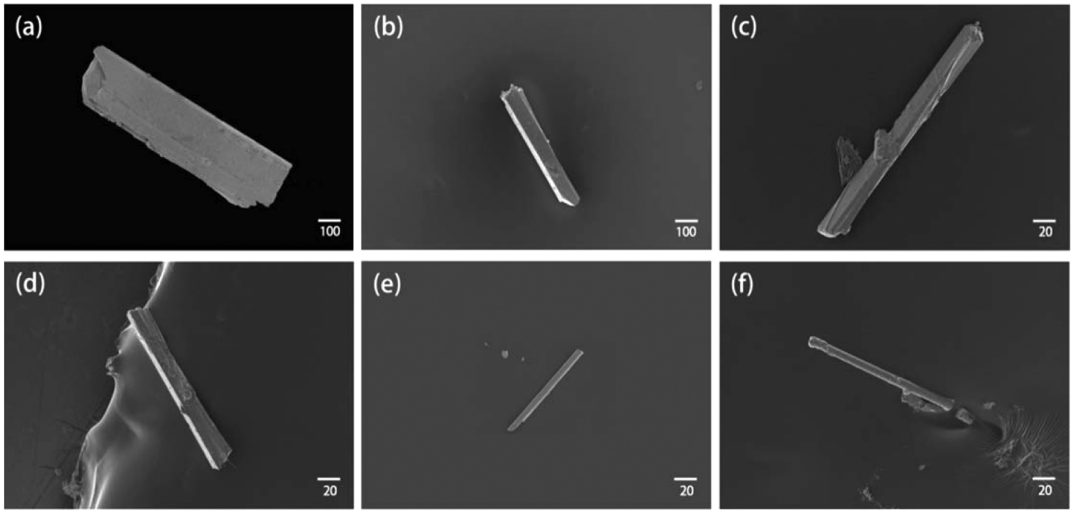

Figure 4. SEM images of bar/needle-shaped single crystals of the Eu-containing compounds with various thicknesses. Scale bars = 100 μm for (a) and (b); and 20 μm for (c)−(f).

edges are capped by In atoms, resulting in a total coordination number of 9.

Single-Crystal Growth and Size Control. Large amounts of bundles having bar/needle-shaped single-crystals of the Eu-containing compounds were obtained out of a metal-flux reaction, where In metals played both roles as a reactant and a solvent. However, the other reaction including Sr atom produced some small cube-shaped single-crystals. Thus, a series of reaction attempts to modify the size of single-crystals was conducted only for the Eu-analogue. During the initial attempt, after the three days of annealing at 500 °C, the sample was centrifuged instantaneously to remove the extra amounts of molten indium metal. The product contained bundles of nicely grown bar/needle-shaped single-crystals with metallic-luster as shown in Figure 4a, and the thickness of the largest crystal was measured ca. 270 μm.

In order to determine whether the size of single crystals can be controlled by adjusting reaction conditions, we have changed three variables, each of which possibly influences the size of products:[22] (1) the annealing duration, (2) the reaction cooling rate, and (3) the centrifugation temperature. The list of reaction attempts with different conditions is shown in Table 4. First, we examined the influence of the annealing duration in reactions 2 and 3 in Table 4 by extending it up to 7 days or by eliminating it completely, respectively. While the influence of extending the annealing duration up to 7 days was insignificant in terms of growing larger or thicker single crystals, the other reaction without the annealing process diminished thicknesses down to ca. 190 μm. These results implied that the duration of the annealing process has already reached its optimum after 3 days at the given reaction condition. However, reducing the process less than 3 days was effective to decrease the thickness. Second, to produce even smaller or thinner single crystals, the reaction cooling rate was doubled from 5 °C/h to 10 °C/h (reaction 4 in Table 4). This attempt successfully resulted in decreasing thicknesses down to ca. 85 μm (Figure 4b). As the cooling rate increased further up to 20 °C/h (reaction 5 in Table 4), 40 °C/h (reaction 6 in Table 4), and 80 °C/h (reaction 7 in Table 4), the overall thicknesses sequentially decreased and eventually came down to ca. 6 μm, which was ca. 45 times thinner than that of the initial reaction (Figure 4c−e). Third, the centrifugation temperature was elevated from 500 °C to 730 °C (reaction 8 in Table 4), which caused the same effect as shortening the cooling duration in the half. Reaction 6 in Table 4 was originally allowed to grow single crystals during the cooling process from 960 °C to 500 °C by 40 °C/h. As the duration of the cooling-process was shortened in half (i.e., centrifugation at 730 °C), the overall crystal sizes became thinner (Figure 4f). Therefore, the series of our reaction attempts proved that the cooling rate and the centrifugation temperature were significantly influential in controlling the size of single crystals.

Table 4. List of Various Reaction Conditions for the Eu-Containing Compounds

reaction	maximum temp. (°C)	dwelling duration (h)	cooling rate (°C/h)	centrifugation temperature (°C)	annealing duration (days)
1	960	20	5	500	3
2	960	20	5	500	7
3	960	20	5	500	
4	960	20	10	500	
5	960	20	20	500	
6	960	20	40	500	
7	960	20	80	500	
8	960	20	40	730	
9	960	20	100	730	

Lastly, we attempted to differentiate two already-proven reaction conditions simultaneously to determine whether the concurrent utilization of two conditions could produce even smaller or thinner single crystals (see reaction 9 in Table 4). For this trial, both of the cooling rate and the centrifugation temperature increased, up to 100 °C/h and 730 °C, respectively. However, the size reduction was insignificant, and the thicknesses were comparable to that of the products from reactions 7 and 8 in Table 4 (ca. 10 μm). Therefore, this attempt proved that the thickness reduction of the bars/needles by adjusting two reaction conditions seemed to reach its limit at ∼10 μm. The further reduction in size, down to the nanometer scale, should be assisted by some types of nanotemplates, such as AAO or SBA.[35,36] These research works are currently under investigation in our group.

dx.doi.org/10.1021/ic500340x | Inorg. Chem. 2014, 53, 4669−4677

Electronic Structure Calculations. Overall features of the electronic structure and individual chemical bonding of the Eu-containing compounds have been interrogated using the TB-LMTO-ASA method.[23d] Since the atomic site having a mixed occupation cannot be applied to this type of theoretical approach,[6,7] the structure model with an idealized composition of "$Eu_3Ca_6In_8Ge_8$" was utilized for the series of calculations in this work. For this model, two cationic sites (M2 and M5), which were proven to contain the largest Eu contents, according to the single-crystal XRD analyses, were assigned solely for Eu, whereas the rest of the cationic sites were occupied only by Ca. Other detail crystallographic data including a space group, lattice parameters, and atomic coordinates for this model also were extracted from the single-crystal XRD results of $Eu_{3.13(2)}Ca_{5.87}In_8Ge_8$.

Total and partial DOS curves of $Eu_3Ca_6In_8Ge_8$ show a valence orbital mixing of four components throughout the entire range of the energy window (Figure 5a). Interestingly, some orbital contributions from two types of cations are observed in the valence band region between −4 eV and 0 eV; this indicates that a certain degree of chemical bonding

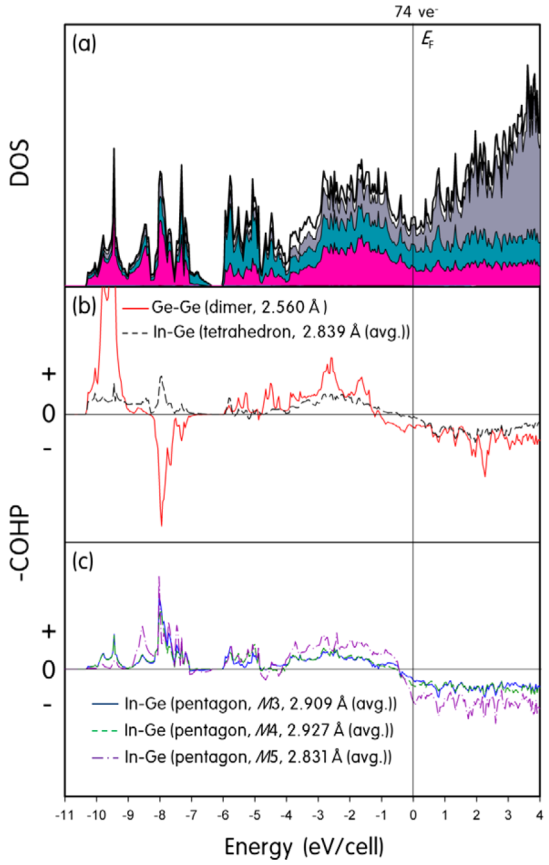

Figure 5. DOS and COHP curves for the idealized model "$Eu_3Ca_6In_8Ge_8$". (a) Total and partial DOS curves are represented by a solid line and shaded areas with different colors as follows: Eu, white; Ca, dark gray; Ge, magenta; and In, green area. E_F (vertical line) is shown as a reference at 0 eV. Individual COHP curves are displayed: (b) Ge−Ge forming a dimer and In−Ge forming a tetrahedron, and (c) In−Ge forming pentagons around M3, M4, and M5 sites, respectively. Average bond distances are also displayed. In the −COHP curves, the positive ("+") values represent bonding interactions, whereas the negative ("−") values represent antibonding interactions, respectively.

interactions between cationic and anionic components should exist. This type of cation participation in chemical bond is one of the typical features observed in many polar intermetallic compounds,[37,38] which is also closely related to the incomplete electron transfer from cations to anions. In addition, this feature results in forming a local DOS minimum (pseudo-gap) at E_F (0 eV) rather than a band gap. Four large DOS peaks are observed between −10 eV and −7 eV, representing the largest orbital contribution from Ge atoms. In particular, two peaks centered at −9.5 and −7.5 eV display, respectively, the σ_s bonding and the σ_s* antibonding interactions of Ge_2 dimers bridging between the 12-membered rings and $InGe_4$ tetrahedra. In addition, some orbital contributions from In 5*s* states of In−Ge interactions forming pentagons and $InGe_4$ tetrahedra are also observed. The region between −6 and 0 eV can roughly be divided into two sectors by another local DOS minimum at ca. −4 eV. Contributions from In 5*p* states and Ge 5*p* states forming pentagons are observed in both sectors, regardless of the bond distances, while those states participating in Ge_2 dimers and $InGe_4$ tetrahedra (average distance of 2.839 Å) contributes more to the higher sector. The region above E_F displays significant contributions from Eu and Ca with some antibonding features descended from various In−Ge and Ge−Ge interactions.

Five COHP curves representing several anionic interactions within the 3D framework are shown in Figures 5b and 5c. In particular, the averaged In−Ge COHP curve for the $InGe_4$ tetrahedron is nearly optimized at E_F, whereas the Ge−Ge COHP curve for the Ge_2 dimer displays a certain degree of antibonding character (Figure 5b). Unlike the In−Ge COHPs for the tetrahedron, those for various pentagonal-prismatic environments present small antibonding characters at E_F (Figure 5c). However, those antibonding characters between anionic components are compensated by relatively weak, but large numbers of bonding interactions between cations and anions (see Figure S2 in the Supporting Information).

To visualize the chemical bond strengths and polarization among anionic elements in the 3D framework, the electron localization function (ELF) and electron density map have been evaluated and plotted in Figure 6. In particular, the ELF diagram is known to represent the paired-electron densities observed in bonding pairs and lone pairs.[39−41] The crystallographic *ac*-plane with y = 0.75 was selected, since the plane included interesting interatomic interactions, such as those of the 12-membered rings and Ge_2 dimers. In both Figures 6a and 6b, the left-half of the diagram illustrates the anionic framework formed by In and Ge, and the right-half displays five cationic sites between the frameworks. Some attractors indicating local ELF maxima are observed between In and Ge atoms forming various pentagons with different interatomic distances between 2.788 and 3.047 Å (Figure 6a). In particular, attractors found between In2−Ge2 and In2−Ge4 bonds are relatively weaker than other attractors observed around the rest of the pentagons, because of the elongated distances of 2.978 and 3.047 Å, respectively (see Table 3). Moreover, the attractors between In and Ge are mostly polarized toward Ge atoms, because of the electronegativity difference between the two elements: In = 1.78 and Ge = 2.01 on the Pauling scale.[34] Figure 6b illustrates the electron density distributions around anionic and cationic elements within the 3D framework and those around cationic sites.

Magnetic Property Measurements. To understand the magnetic characteristics of Eu atoms located at five different

dx.doi.org/10.1021/ic500340x | Inorg. Chem. 2014, 53, 4669−4677

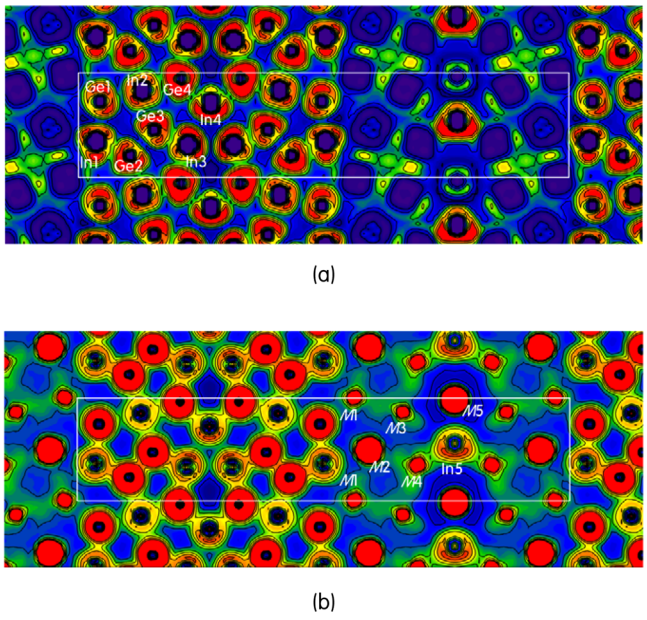

Figure 6. (a) Electron localization function (ELF) diagram and (b) electron density map calculated for the idealized model "$Eu_3Ca_6In_8Ge_8$". Two diagrams display the *ac*-plane with $y = 0.75$ and are depicted as filled and line contour maps. The color scheme ranges from blue to red (0–0.8) for ELF, and values higher than 0.5 represent the area exceeding free-electron ELF values. Unit cell is outlined in both diagrams.

cationic sites in $Eu_{3.13(2)}Ca_{5.87}In_8Ge_8$, the isofield magnetization as a function of temperature and the isothermal magnetization as a function of magnetic field were evaluated on a polycrystalline specimen.

Figure 7a displays the magnetization as a function of temperature between 4 K and 300 K using ZFC and FC conditions under the dc magnetic field of 10 kOe. The inset shows a temperature-dependent inverse dc magnetic susceptibility. $Eu_{3.13(2)}Ca_{5.87}In_8Ge_8$ shows typical Curie–Weiss behavior in the corresponding paramagnetic region above ca. 150 K, given the localized *f* electrons, and there exists no clear indication of magnetic ordering down to 4 K. The effective magnetic moment obtained from a linear fit of the inverse magnetic susceptibility versus temperature is 7.12 μ_B per Eu atom, and this value is lower than the theoretically expected effective magnetic moment of 7.94 μ_B for a free Eu^{2+} ion. The discrepancy between observed and theoretical values should mainly be attributed to In metals remaining in the product, even after the centrifugation, acting like a glue between single crystals to hold them together, resulting in the formation of bundles of bars/needles of products. Peaks descended from the remaining In metals were indexed in the power diffraction pattern shown in Figure S1 in the Supporting Information. In addition, small amounts of Eu_2O_3 impurity observed on the surface of crystals should also be influential to the reduced effective magnetic moment. The extrapolation of the linear fitting for the magnetic susceptibility curve in the paramagnetic region results in $\theta_P = -2.58$ K, which implies a relatively low temperature antiferromagnetic (AFM) ordering of Eu atoms in $Eu_{3.13(2)}Ca_{5.87}In_8Ge_8$. Figure 7b displays magnetization as a function of magnetic field between −70 and 70 kOe at 4 K. The maximum magnetization of ca. 4.6 μ_B per Eu atom is observed at 70 kOe, which is considerably lower than the theoretically predicted saturated magnetization of 7 μ_B for the free Eu^{2+}.

CONCLUSION

Three novel polar intermetallic compounds—$Eu_{2.94(2)}Ca_{6.06}In_8Ge_8$, $Eu_{3.13(2)}Ca_{5.87}In_8Ge_8$, and $Sr_{3.23(3)}Ca_{5.77}In_8Ge_8$—have been synthesized, using molten indium metal as a reactive flux. Bundles of well-grown bar/needle-shaped single crystals were obtained from the Eu-containing compounds, whereas small cube-shaped single crystals were produced from the Sr-containing product. The thicknesses of single crystals of the Eu compounds were successfully controlled in the micrometer scale by adjusting two reaction conditions: the reaction cooling-rate and the centrifugation temperature. The novel structure type was characterized by both powder and single-crystal X-ray diffraction analyses, and the overall crystal structure can be described as a combination of two basic structural components: (1) the three-dimensional (3D) polyanionic framework consisting of the 12-membered rings and the $InGe_4$ tetrahedra, and (2) the mixed-cationic sites filling the voids between the 3D frameworks. All five cationic sites are composed of the mixed occupations of Eu (or Sr) and Ca with various atomic

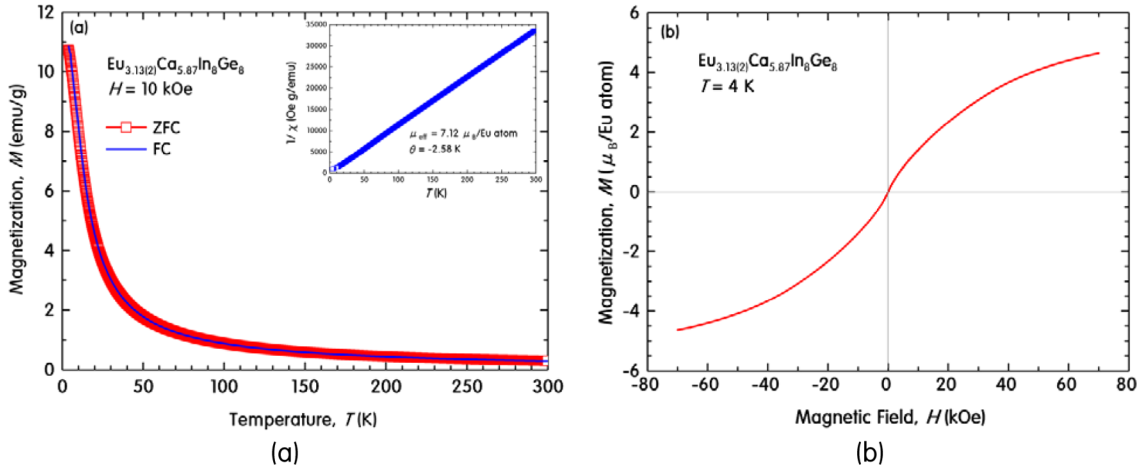

Figure 7. (a) Temperature-dependent magnetization of $Eu_{3.13(2)}Ca_{5.87}In_8Ge_8$ measured in dc magnetic field of 10 kOe under both ZFC and FC conditions. Inset displays the linear fit of temperature-dependent inverse magnetic susceptibility measured in 10 kOe under the FC condition. (b) Magnetization in the Bohr magnetron (μ_B) as a function of the magnetic field measured at 4 K.

dx.doi.org/10.1021/ic500340x | Inorg. Chem. 2014, 53, 4669–4677

ratios, and three of the title compounds were obtained only when both types of cations coexist in the crystal structure. Overall crystal sizes of the Eu compounds can be controlled by either speeding-up the cooling rate or increasing the centrifugation temperature, and the thickness of bar/needle-shaped single-crystals was successfully reduced down to ca. 6 μm. However, the further size-reduction down to the nanometer scale should be achieved with a help of some types of nanotemplates. TB-LMTO-ASA calculations were conducted on a model structure of $Eu_3Ca_6In_8Ge_8$, and density of states (DOS) analysis indicated some orbital interactions between cations and anions resulting in a semimetallic property. Crystal orbital Hamilton population (COHP) curves proved that In−Ge interactions in both tetrahedral- and pentagonal-coordination environments were optimized or at least nearly optimized at the Fermi energy (E_F), whereas a COHP curve for the Ge_2 dimer displayed some antibonding characters, which were eventually compensated by bonding characters of interatomic interactions between cations and anions. The electron localization function (ELF) diagram illustrated bond strengths and polarization among anions within the 3D framework. Magnetic susceptibility measurements for $Eu_{3.13(2)}Ca_{5.87}In_8Ge_8$ proved a divalent state of Eu atoms with an effective magnetic moment of 7.12 μ_B per Eu atom, and the extrapolation of the linear fitting for the paramagnetic region implied a relatively low AFM ordering temperature (T_N < 4 K) of Eu atoms with θ_P = −2.58 K.

■ ASSOCIATED CONTENT

Supporting Information

Three single-crystal X-ray crystallographic CIF files, a powder X-ray diffraction pattern of $Eu_{3.13(2)}Ca_{5.87}In_8Ge_8$, and five COHP curves representing different cation−anion interactions. This material is available free to charge via the Internet at http://pubs.acs.org.

■ AUTHOR INFORMATION

Corresponding Author

*E-mail: tsyou@chungbuk.ac.kr.

Notes

The authors declare no competing financial interest.

■ ACKNOWLEDGMENTS

This work is supported by Basic Science Research Program through the National Research Foundation of Korea (NRF) funded by the Ministry of Education, Science and Technology (Grant No. 2012010941).

■ REFERENCES

(1) Kanatzidis, M. G.; Pöttgen, R.; Jeitschko, W. *Angew. Chem., Int. Ed.* **2005**, *44*, 6996−7023.
(2) Phelan, W. A.; Menard, M. C.; Kangas, M. J.; McCandless, G. T.; Drake, B. L.; Chan, J. Y. *Chem. Mater.* **2012**, *24*, 409−420.
(3) Bugaris, D. E.; zur Loye, H. C. *Angew. Chem., Int. Ed.* **2012**, *51*, 3780−3811.
(4) Tobash, P. H.; Lins, D.; Bobev, S.; Lima, A.; Hundley, M. F.; Thompson, J. D.; Sarro, J. L. *Chem. Mater.* **2005**, *17*, 5567−5573.
(5) Tobash, P. H.; Lins, D.; Bobev, S. *Inorg. Chem.* **2006**, *45*, 7286−7294.
(6) You, T.-S.; Tobash, P. H.; Bobev, S. *Inorg. Chem.* **2010**, *49*, 1773−1783.
(7) You, T.-S.; Bobev, S. *J. Solid State Chem.* **2010**, *183*, 1258−1265.
(8) Oliynyk, A. O.; Stoyko, S. S.; Mar, A. *Inorg. Chem.* **2013**, *52*, 8264−8271.
(9) Oliynyk, A. O.; Mar, A. *J. Solid State Chem.* **2013**, *206*, 60−65.
(10) Sarkar, S.; Peter, S. *Inorg. Chem.* **2013**, *52*, 9741−9748.
(11) Ma, X.; Lu, J.; Whalen, J. B.; Latturner, S. E. *Inorg. Chem.* **2013**, *52*, 3342−3348.
(12) Subbarao, U.; Sebastian, A.; Rayaprol, S.; Yadav, C. S.; Svane, A.; Vaitheeswaran, G.; Peter, S. C. *Cryst. Growth Des.* **2013**, *13*, 352−359.
(13) Ribeiro, R. A.; Avila, M. A. *Philos. Mag.* **2012**, *92*, 2492−2507.
(14) Mahjoor, P.; Latturner, S. E. *Philos. Mag.* **2012**, *92*, 2582−2595.
(15) West, J. P.; Hwu, S. J. *J. Solid State Chem.* **2012**, *195*, 101−107.
(16) Shannon, R. D. *Acta Crystallogr., Sect. A: Cryst. Phys. Diffr., Theor. Gen. Crystallogr.* **1976**, *32*, 751−767.
(17) Sumanta, S.; Matthias, J. G.; Sebastian, C. P. *Cryst. Growth Des.* **2013**, *13*, 4285−4294.
(18) Klem, M. T.; Vaughy, J. T.; Harp, J. G.; Corbett, J. D. *Inorg. Chem.* **2001**, *40*, 7020−7026.
(19) Bobev, S.; Bauer, E. D.; Thompson, J. D.; Sarrao, J. L.; Miller, G. J.; Eck, B.; Dronskowski, R. *J. Solid State Chem.* **2004**, *177*, 3545−3552.
(20) You, T.-S.; Grin, Y.; Miller, G. J. *Inorg. Chem.* **2007**, *46*, 8801−8811.
(21) You, T.-S.; Lidin, S.; Gourdon, O.; Wu, Y. Q.; Miller, G. J. *Inorg. Chem.* **2009**, *48*, 6380−6390.
(22) Ozawa, T. C.; Kauzlarich, S. M. *J. Cryst. Growth* **2004**, *265*, 571−576.
(23) (a) Andersen, O. K. *Phys. Rev. B* **1975**, *12*, 3060−3083. (b) Andersen, O. K.; Jepsen, O. *Phys. Rev. Lett.* **1984**, *53*, 2571−2574. (c) Andersen, O. K. *Phys. Rev. B* **1986**, *34*, 2439−2449. (d) Jepsen, O.; Burkhardt, A.; Andersen, O. K. *The TB-LMTO-ASA Program*, version 4.7; Max-Plank-Institut für Festkorperforschung: Stuttgart, Germany, 1999. (e) Andersen, O. K.; Jepsen, O.; Glötzel, D. In *Highlights of Condensed Matter Theory*; Bassani, F., Fumi, F., Tosi, M., Eds.; North-Holland: New York, 1985.
(24) Dronskowski, R.; Blöchl, P. *J. Phys. Chem.* **1993**, *97*, 8617−8624.
(25) Hunter, B. A. In *Commission for Powder Diffraction Newsletter*, No. *20*; International Union of Crystallography, Oak Ridge, TN, 1998; p 21.
(26) *APEX2*; Bruker Analytical X-ray Systems, Inc.: Madison, WI, 2007.
(27) *SAINT*; Bruker Analytical X-ray Systems, Inc.: Madison, WI, 2002.
(28) Sheldrick, G. M. *SADABS*, University of Göttingen: Göttingen, Germany, 2003.
(29) Sheldrick, G. M. *SHELXTL*; University of Göttingen: Göttingen, Germany, 2001.
(30) Gelato, L. M.; Parthe, E. *J. Appl. Crystallogr.* **1987**, *20*, 139−143.
(31) Jepsen, O.; Andersen, O. K. *Z. Phys. B* **1995**, *97*, 35−47.
(32) Blöchl, P. E.; Jepsen, O.; Andersen, O. K. *Phys. Rev. B* **1994**, *49*, 16223−16233.
(33) Salvador, J. R.; Kanatzidis, M. G. *Inorg. Chem.* **2006**, *45*, 7091−7099.
(34) Emsley, J. *The Elements*; Clarendon Press: Oxford, U.K., 1990.
(35) Zhixun, L.; Yan, F.; Xiaofang, Z.; Jiannian, Y. *Mater. Chem. Phys.* **2008**, *107*, 91−95.
(36) Lai, C. C.; Lin, Y. K.; Yuan, F. W.; Tuan, H. Y.; Chueh, Y. L. *ECS Solid State Lett.* **2013**, *2*, 55−57.
(37) Mudring, A.-V.; Corbett, J. D. *J. Am. Chem. Soc.* **2004**, *126*, 5277−5281.
(38) Miller, G. J.; Lee, C.-S.; Choe, W. In *Inorganic Chemistry Highlights*; Meyer, G., Naumann, D., Wesemann, L., Eds.; Wiley−VCH: Berlin, 2002.
(39) Savin, A.; Flad, H. J.; Preuss, H.; von Schnering, H. G. *Angew. Chem.* **1992**, *104*, 185−186. Savin, A.; Flad, H. J.; Preuss, H.; von Schnering, H. G. *Angew. Chem., Int. Ed. Engl.* **1992**, *31*, 185−187.
(40) (a) Kohout, M. *Int. J. Quantum Chem.* **2004**, *97*, 651−658. (b) Kohout, M.; Wagner, F. R.; Grin, Yu. *Theor. Chem. Acc.* **2002**, *108*, 150−156.
(41) Gatti, C. *Z. Kristallogr.* **2005**, *220*, 399−457.